Imaging Properties of Off-Axis Parabolic Mirrors

J. Howard

June 1977

UWFDM-214

FUSION TECHNOLOGY INSTITUTE

UNIVERSITY OF WISCONSIN

MADISON WISCONSIN

Imaging Properties of Off-Axis Parabolic Mirrors

J. Howard

Fusion Technology Institute
University of Wisconsin
1500 Engineering Drive
Madison, WI 53706

http://fti.neep.wisc.edu

June 1977

UWFDM-214

"LEGAL NOTICE"

"This work was prepared by the University of Wisconsin as an account of work sponsored by the Electric Power Research Institute, Inc. ("EPRI"). Neither EPRI, members of EPRI, the University of Wisconsin, nor any person acting on behalf of either:

"a. Makes any warranty or representation, express or implied, with respect to the accuracy, completeness, or usefulness of the information contained in this report, or that the use of any information, apparatus, method, or process disclosed in this report may not infringe privately owned rights; or

"b. Assumes any liabilities with respect to the use of, or for damages resulting from the use of, any information, apparatus, method or process disclosed in this report."

Imaging Properties of Off-Axis Paraboiic Mirrors

James E. Howard
University of Wisconsin, Nuclear Engineering Department
Madison, Wisconsin 53706

Abstract

Geometric optics is used to find the shape of the image and the irradiance cast on a spherical target by a circular beam after reflection by a far off-axis paraboloidal mirror. For moderately large f/no. the image is found to be nearly circular with its center shifted slightly from the beam axis. However, the target irradiance can be highly asymmetric unless the beam intensity falls off rapidly with radius. An expansion in powers of inverse f/no. is used to obtain closed form expressions for the image shape and the target irradiance. Numerical studies are carried out for parameters relevant to the design of a laser fusion reactor. Limits are placed on allowable tilt errors by means of a naive analysis of ray aberrations. A useful formula is derived for the perturbed target irradiance under small tilt errors, based on a new expression for the caustic. These simple formulas allow one to carry out detailed design studies without recourse to ray tracing codes.

I. Introduction

Off-axis parabolic mirrors are widely used in astronomy and laser fusion experiments for simultaneously deflecting and focusing a collimated beam.[1] Traditionally difficult to fabricate, their use has become much more economical with the advent of the diamond-turning technique.[2] In this paper, geometric optics is employed to obtain analytical expressions for the shape of the image and the irradiance cast on a spherical target by a circular beam. (The target is assumed to be large enough that diffraction effects may be ignored). For moderately large f/no. the reflected beam is found to be nearly circular, with its geometric center shifted by a small amount from the beam axis. The target irradiance, on the other hand, can be highly asymmetric unless the beam intensity falls off rapidly at the beam edge. An expansion in powers of inverse f/no. is used to obtain closed form expressions for the image shape and target irradiance. Numerical calculations are carried out for parameters relevant to the design of a laser fusion reactor.

Since proposed laser fusion reactor targets are small ($\sim$ 1 mm) and focal lengths long[3,4] ($\gtrsim$ 10 m), pointing errors must be held to about one arcsecond. Conventional analysis of Seidel aberrations is limited to regions near the optical axis of

axisymmetric systems, and does not apply to far off-axis rays.[5] Nevertheless, since spherical aberration is absent at all ray heights, one may readily calculate aberrations due to various tilt errors. This is done analytically in Sec. IV. An expression is derived for the perturbed target irradiance under small tilt errors, based on a new calculation of the caustic curve. These simple formulas allow one to carry out detailed design studies without recourse to ray tracing codes.

Figure 1 depicts a circular beam of radius ρ_B incident on an off-axis portion of a parabolic mirror such that the beam axis is turned (deflected) through an angle ϕ_0 and the effective focal distance measured along the beam axis is r_0. A paraboloid of revolution may be described in cylindrical coordinates by

$$R^2 = 4a(a-z) \tag{1}$$

and in spherical polar coordinates by

$$r = \frac{2a}{1+\cos\phi} = a \sec^2(\phi/2) , \tag{2}$$

where a is the paraxial focal length of the complete paraboloid. The distance 4a is then the latus rectum. Here z is measured to the left of O' in order that the turning angle ϕ be the spherical polar angle. The distance from ray to axis is then

$$R = \frac{2a\sin\phi}{1+\cos\phi} = 2a \tan(\phi/2) . \tag{3}$$

We shall refer to the symmetry plane $\theta = 0$ as the median plane.

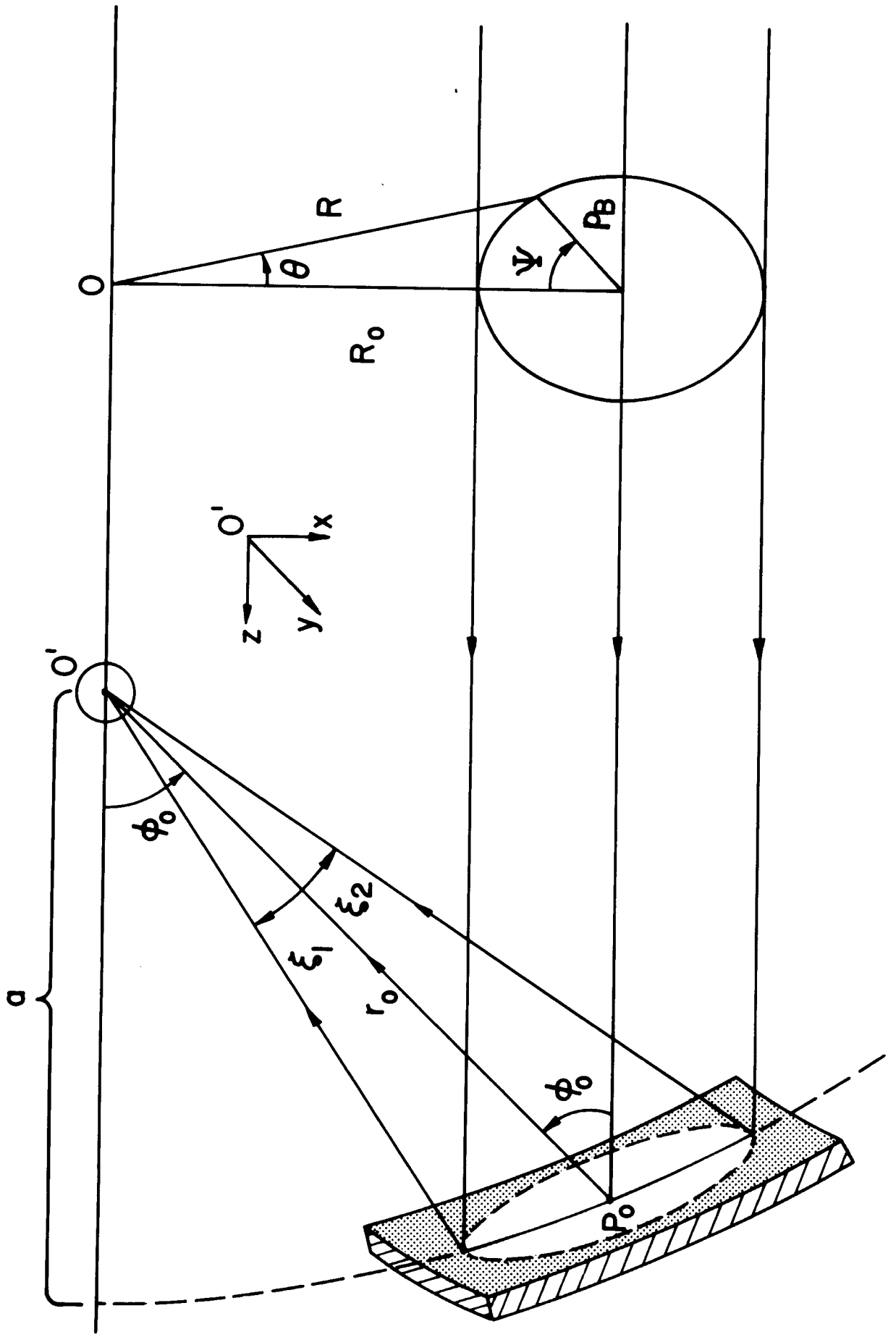

Figure 1

II. Image Mapping

We wish to find the shape of the image and the irradiance distribution on a small ($R_T \simeq 1$ mm) spherical target and the image outline at some distance from the target, where the beam ports are to be placed. Figure 2 depicts the image of a circular beam in a plane normal to $\vec{r}_o$, at an arbitrary distance $r_o^* < r_o$ from the focus. Let us identify a point P on the edge of the object disk by polar coordinates (ρ_B,Ψ) and its image P' in a plane normal to $\vec{r}_o^*$ by (ρ',Ψ'). The polar coordinates of point P with respect to the origin at the focus O are

$$R^2 = R_o^2 + \rho_B^2 - 2R_o\rho_B \cos\Psi \tag{4}$$

$$\sin\theta = \frac{\rho_B}{R} \sin\Psi \ . \tag{5}$$

The reflected ray $\vec{r}(r,\theta,\phi)$ is then determined by Eqs. (2), (3) and (5). In most laser fusion reactor applications the spot size is sufficiently small that the angle ξ may be used in place of the distance $\rho' = r_o^* \tan\xi$ in measuring port radii.

The angles ξ and Ψ' in Fig. 2 locate the vector $\vec{r}$ with respect to a rotated spherical polar coordinate system having its z axis along $\vec{r}_o$, as shown in Fig. 3. (We have reversed the sense of $\vec{r}$ and $\vec{r}_o$ relative to Fig. 1). Rotating the z axis through the angle ϕ_o in the x-z plane, the new coordinates of $\vec{r}$ are

$$\tilde{x} = x\cos\phi_o - z\sin\phi_o = r\sin\xi\cos(\pi-\Psi') \tag{6}$$

$$\tilde{y} = y = r\sin\xi\sin(\pi-\Psi')$$

$$\tilde{z} = x\sin\phi_o + z\cos\phi_o = r\cos\xi \ ,$$

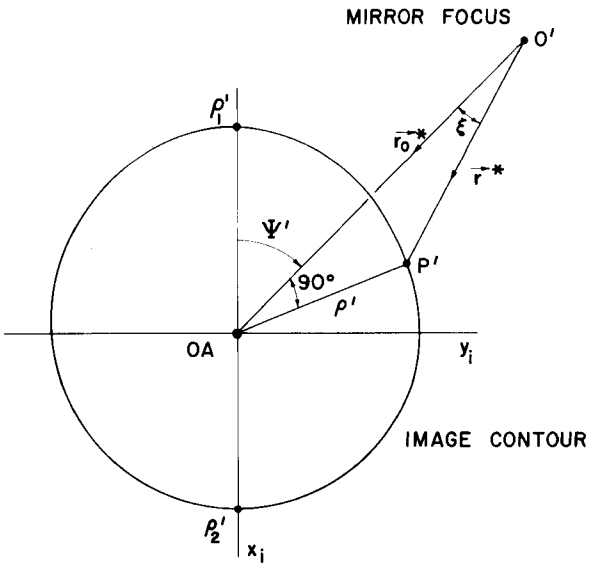

Figure 2

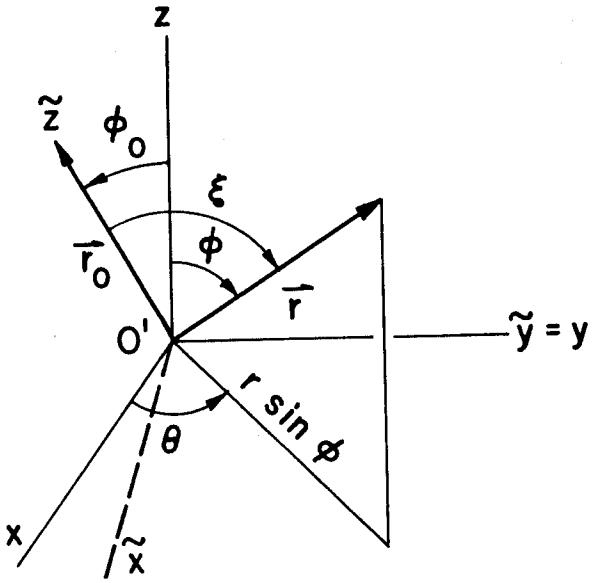

Figure 3

where

$$x = r \sin\phi \cos\theta \tag{7}$$

$$y = r \sin\phi \sin\theta$$

$$z = r \cos\phi \ .$$

Thus,

$$\cos\xi = \sin\phi_o \sin\phi \cos\theta + \cos\phi_o \cos\phi \tag{8}$$

$$\tan\psi' = \frac{\sin\phi \sin\theta}{\sin\phi_o \cos\phi - \cos\phi_o \sin\phi \cos\theta} \tag{9}$$

$$\sin\xi \sin\psi' = \sin\phi \sin\theta \ . \tag{10}$$

Any pair of Eqs. (8)-(10) determine the image in beam-centered coordinates. It is useful to introduce the smallness parameter (essentially inverse off-axis f/no.)

$$\varepsilon \equiv \rho_B / r_o \ . \tag{11}$$

Eqs. (8)-(10) may then be expanded in powers of ε to obtain

$$\psi' = \psi + \frac{1}{2} \varepsilon \sin\psi \tan(\phi_o/2) + O(\varepsilon^2) \tag{12}$$

$$\xi = \varepsilon + \frac{1}{2} \varepsilon^2 \cos\psi \tan(\phi_o/2) + O(\varepsilon^3) \ , \tag{13}$$

where terms of order ε^2 and ε^3 have been omitted.

It follows that

$$\xi^2 \sin^2\psi' + (\xi\cos\psi' - \Delta\xi)^2 = \varepsilon^2 + O(\varepsilon^4) \ , \tag{14}$$

where

$$\Delta\xi \equiv \frac{1}{2}\,\varepsilon^2 \tan(\phi_o/2) \ . \tag{15}$$

That is, to lowest order the image is circular with its center shifted through the angle $\Delta\xi$ in the median plane from the beam axis in the $-\phi$ direction as depicted in Fig. 4. Higher order contributions to ξ and ψ' are very tedious to calculate.

The angles ξ_1 and ξ_2 delimiting the spot size in the median plane are then (Fig. 1)

$$\xi_{1,2} = \varepsilon(1 \pm \frac{1}{2}\,\varepsilon \tan(\phi_o/2)) \ . \tag{16}$$

The following semi-empirical formula is more accurate:

$$\xi_{1,2} = \varepsilon(1 \mp \frac{1}{2}\,\varepsilon \tan(\phi_o/2))^{-1} \ . \tag{17}$$

Since the image is nearly circular, it makes sense to define an effective off-axis f/no. from $\bar{\xi} = (\xi_1 + \xi_2)/2$;

$$F = \frac{1}{2}\cot\bar{\xi} \simeq \frac{1}{2\varepsilon} \ , \tag{18}$$

<u>independent of ϕ_o</u>.

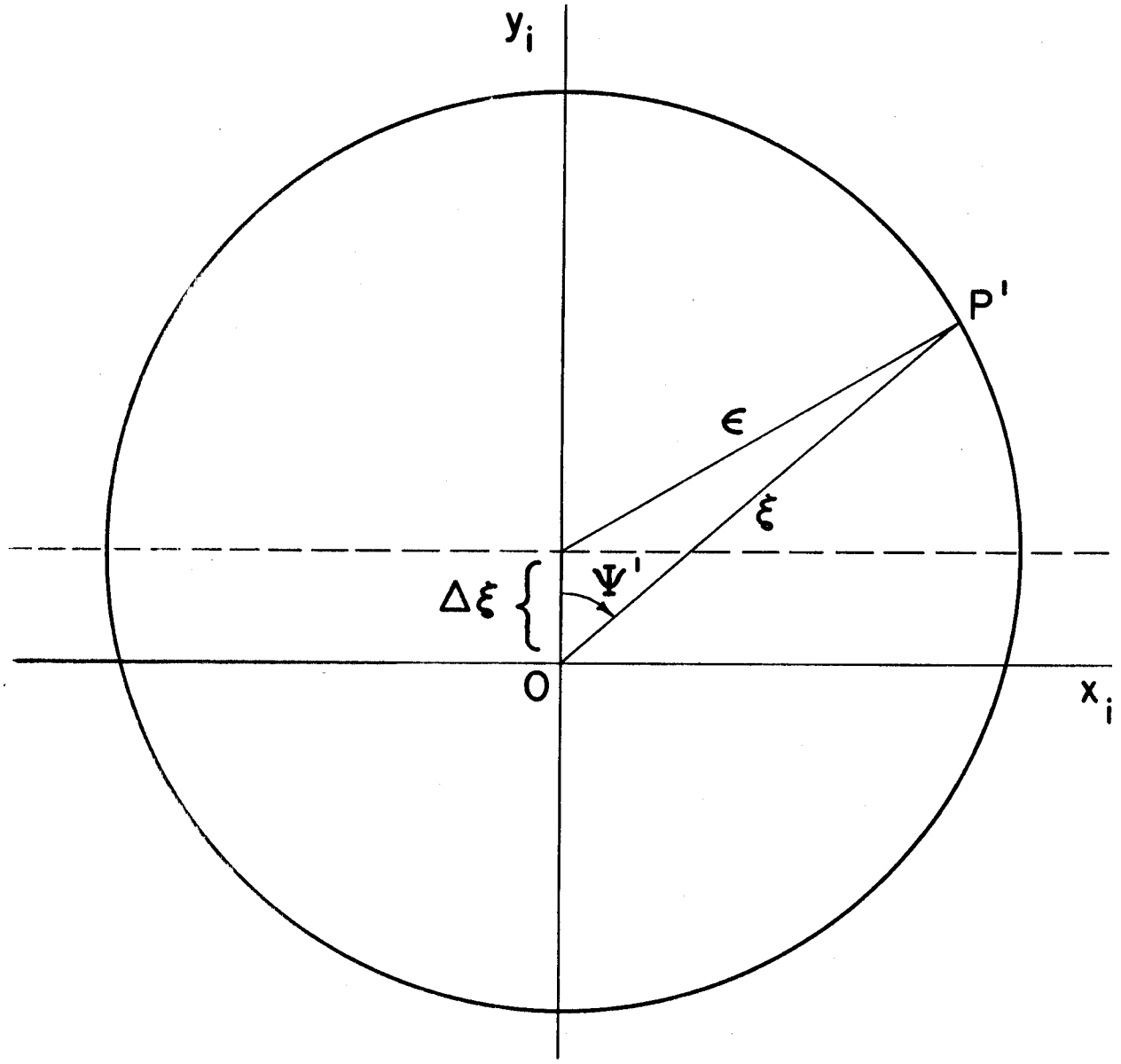

Figure 4

Equations (17) and (18) are accurate to 0.3% for $\varepsilon \leq 0.2$ and $\phi_0 \leq 135^0$. As an important physical consequence, note that an auxiliary beam used to align the beam axis will not pass through the center of the beam port. When $\phi_0 = 90^0$ it may be shown that ξ_1 and ξ_2 are given by the exact formulas,

$$\tan\xi_1 = \varepsilon \left(\frac{1-\varepsilon/2}{1-\varepsilon}\right) \tag{19}$$

$$\tan\xi_2 = \varepsilon \left(\frac{1+\varepsilon/2}{1+\varepsilon}\right) \tag{20}$$

in agreement with Eq. (16) to $O(\varepsilon^2)$. Typical laser fusion reactor parameters are $r_0 = 10$ m, $\rho_B = 1$ m and $\phi_0 = 90^0$, for which $\xi_1 = 6.03^0$, $\xi_2 = 5.43^0$ and $F = 5$.

III. Two-Dimensional Irradiance Profiles

The target and beam irradiances are related by conservation of energy;

$$I_T dA_T = I_B dA_B \ , \tag{21}$$

where (Fig. 1)

$$dA_B = RdRd\theta \tag{22}$$

$$dA_T = R_T^2 \sin\phi \, d\phi d\theta \ . \tag{23}$$

Thus

$$I_T = \frac{I_B(\rho)RdR}{R_T^2 \sin\phi d\phi} \ , \tag{24}$$

where $0 < \rho < \rho_B$. From Eq. (3),

$$\sin\phi \, dR = R d\phi \ , \tag{25}$$

so that

$$I_T = \left(\frac{2a}{R_T}\right)^2 \frac{I_B(\rho)}{(1+\cos\phi)^2} \ . \tag{26}$$

Irradiance profiles are shown in Figs. 5-7 for an off-axis focal length $r_o = 5$ m and a beam radius $\rho_B = 1$ m. $I(\xi)$ is given in the meridional plane (along the x_i axis) for turning angles $\phi_o = 45^o$, 90^o and 135^o, normalized to unity at $\xi = 0$. The beam profiles used were flat and Gaussian;

$$I_B(\rho) = I_o \, e^{-\alpha(\rho/\rho_B)^2} \tag{27}$$

with $\alpha = 1$ and 2. The flat profile results are seen to be highly skewed, worsening with decreasing r_o and increasing ϕ_o. The asymmetry is much less severe, however, for the Gaussian profiles, especially for the case $\alpha = 2$. The reason for this improvement is that the largest distortion, occurring at the beam

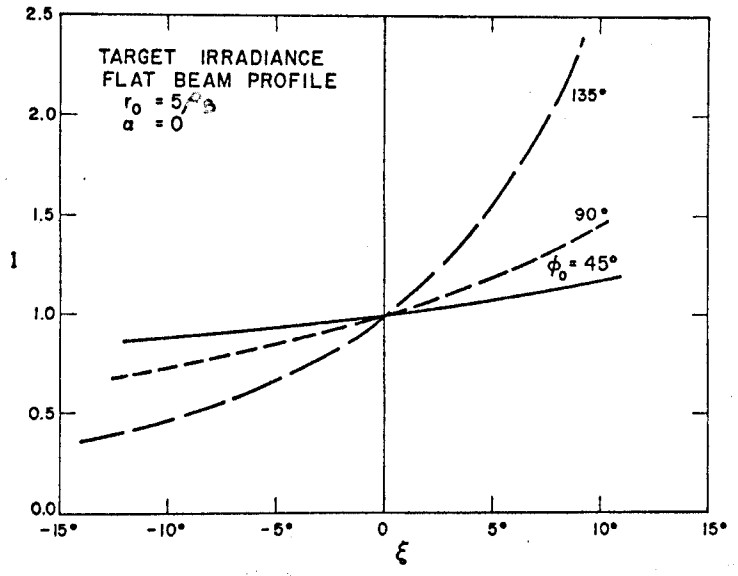
TARGET IRRADIANCE
FLAT BEAM PROFILE
$r_0 = 5\rho_B$
$\alpha = 0$
135°
90°
$\phi_0 = 45°$
I
ξ
2.5
2.0
1.5
1.0
0.5
0.0
-15°
-10°
-5°
0
5°
10°
15°

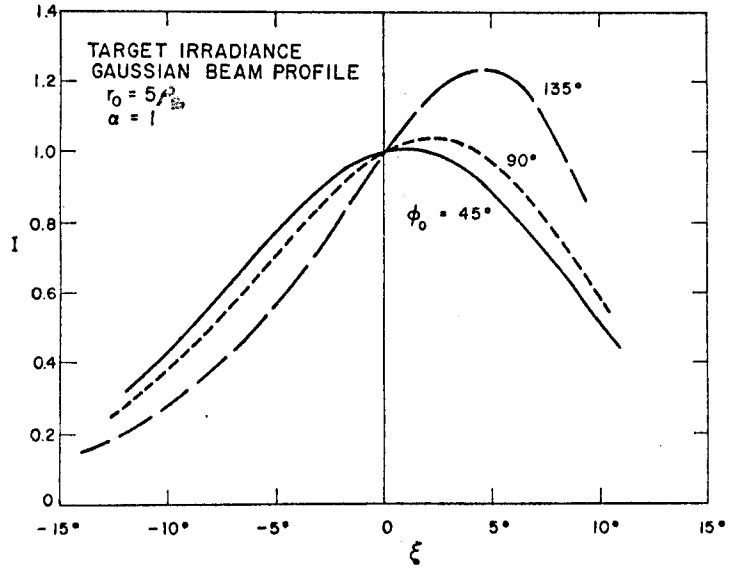
TARGET IRRADIANCE
GAUSSIAN BEAM PROFILE
$r_0 = 5\rho_B$
$\alpha = 1$
135°
90°
$\phi_0 = 45°$
I
ξ
1.4
1.2
1.0
0.8
0.6
0.4
0.2
0
-15°
-10°
-5°
0
5°
10°
15°

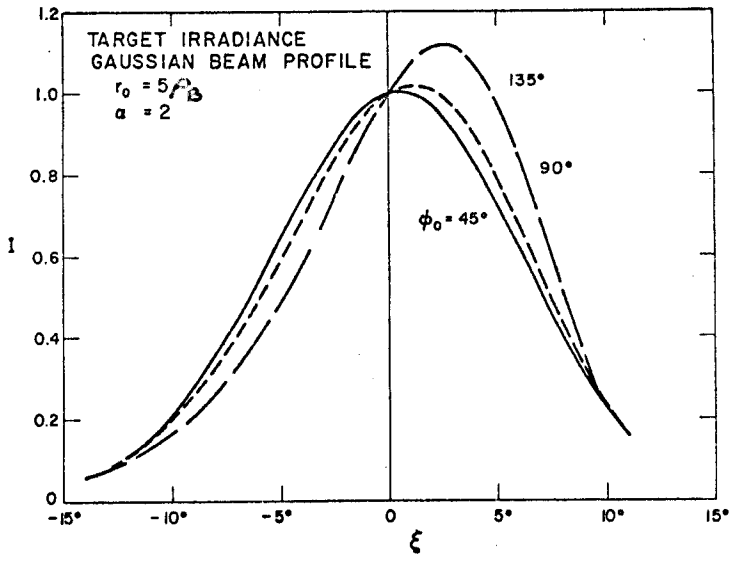
TARGET IRRADIANCE
GAUSSIAN BEAM PROFILE
$r_0 = 5\rho_B$
$\alpha = 2$
135°
90°
$\phi_0 = 45°$
I
ξ
1.2
1.0
0.8
0.6
0.4
0.2
0
-15°
-10°
-5°
0
5°
10°
15°

FIGURES 5-7

edge, is scaled down by the rapidly decreasing Gaussian. The required symmetry depends on the details of the target design. Detailed parameter studies[6] show that quite symmetric irradiances obtain for $r_o \geq 10\ \rho_B$ and $\phi_o \leq 90^o$, using paraboloidal mirrors alone as final focusing elements.

Again taking advantage of the smallness of ξ, one may obtain an explicit formula for $I(\xi)$ along the x_i axis. The result is, in normalized form,

$$I_T(\xi) \simeq [1 + 2t\xi + \frac{1}{2}(1 + 5t^2)\xi^2] \quad \exp\ [-\alpha(\xi/\varepsilon)^2\ (1 + t\xi)] \qquad (28)$$

where $t = \tan(\phi_o/2)$ and $-\xi_1 < \xi < \xi_2$.

IV. Mirror Positioning and Pointing Errors

Illuminating a 1 mm radius target from a distance of 10 m or more with a large off-axis paraboloid and keeping it on target is a formidable technical task. Six degrees of freedom must be controlled in an explosive environment. Further, it is not clear how feedback control can be accomplished or how often corrections would have to be made. Current large scale laser fusion experiments allow hours between shots for alignment, as compared to perhaps 50 msec between pulses in a reactor.[3]

In this section analytic ray tracing is employed to calculate tolerances on each of the six positioning coordinates for arbitrary values of ϕ_o, r_o, ρ_B, and R_T. In each case we assume a stationary

target and collimated beam, allowing only motions of the mirror.

A. Translational Positioning Errors

Any purely translational error δx, δy or δz preserves the parallel relation between the incident ray and the axis of the paraboloid. Consequently, the focal point simply follows the displacement without magnification or confusion of the focal region. Since stepping motors capable of 0.5 μm motions are in existence today,[7] translational errors should not be problematical.

B. Rotational Positioning Errors

Consider rotations about the x, y and z axes with origin at the intersection of the beam axis with the mirror. As the ray displacements on target are proportional to the focal distance r_o, such errors can be quite serious.

1. Rotation About the y_m-axis ($\delta\phi$)

Figure 8 shows the deflection of the principal ray (or any ray in the median plane $\theta = 0$). Simple triangulation yields the axial aberration,

$$\delta z = r \frac{\sin(2\delta\phi)}{\sin\phi'} \simeq \frac{2r\delta\phi}{\sin\phi} \quad . \tag{29}$$

The angle of incidence α and target central angle β are given by

$$\sin\alpha = \frac{\delta z}{R_T} \sin\phi' \simeq \frac{2r\delta\phi}{R_T} \tag{30}$$

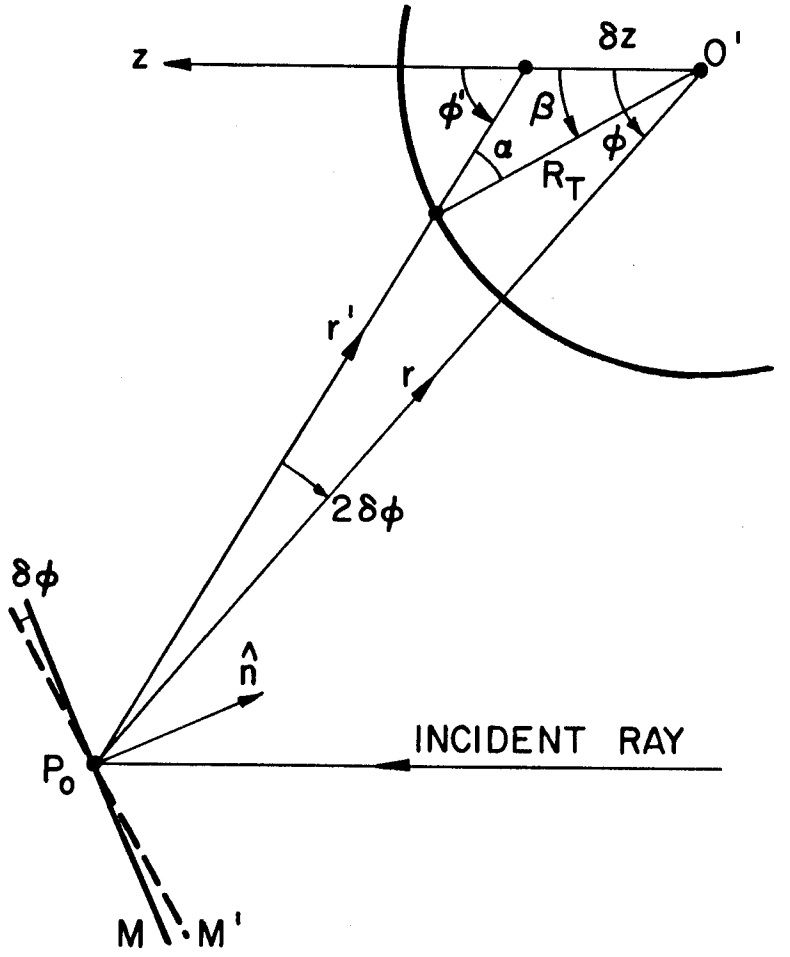

Figure 8

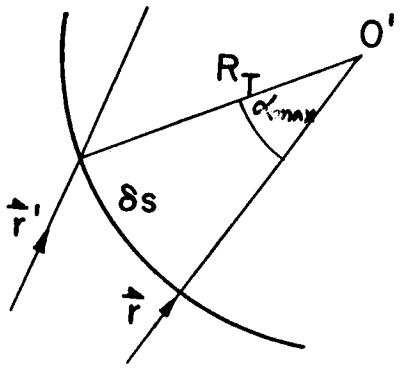

Figure 9

$$\beta = \phi' - \alpha \simeq \phi - \alpha \ , \qquad r >> R_T \ . \tag{31}$$

It can be shown that the deflection of meridional rays out of the median plane differ by terms proportional to θ, which we have assumed to be small. Similarly, when $\Delta\phi = \phi - \phi_o << \phi_o$ it follows from Eq. (29) that a general ray lying in the median plane is deflected by

$$\delta z = \delta z_o \left[1 + \left(\frac{1-2\cos\phi_o}{\sin\phi_o}\right) \Delta\phi\right] \ , \tag{32}$$

where δz_o is the deflection of the principal ray. Since $\Delta\phi \leq \xi \simeq \varepsilon$, the fanning of the rays (corresponding to classical coma and astigmatism) is seen to be negligible. Eq. (32) points out the curious fact that ray fanning is a second order effect when $\phi_o = 60^o$. While ray fanning is unimportant for tilt error control, it does markedly affect the irradiance on the pellet surface, as we shall see in the next section.

Rather than impose a limit on the axial aberration δz, we choose to require that the arc length displacement δs be less than a specified fraction of the pellet circumference (Fig. 9). Since $\delta s \simeq \alpha R_T$, this is equivalent to limiting the angle $\phi - \beta \simeq \alpha$. From Eq. (30),

$$\delta\phi \leq \frac{R_T \sin\alpha_{max}}{2r_o} \ . \tag{33}$$

The precise value of α will depend on the particular pellet design. As an upper bound on α we have the condition to just miss the pellet, $\alpha = 90^{o}$, for which

$$\delta\phi_{max} = R_T/2r_o \ . \tag{34}$$

The deflection of a general ray, for which $\theta \neq 0$, is complicated by the fact that the axis of rotation is no longer normal to the local meridional plane, with the result that the reflected ray does not lie in the unperturbed meridional plane. That is, $\theta \neq$ constant for the perturbed ray. This calculation has been carried out, with negligible difference from Eq. (34), owing to the smallness of θ.

2. Rotation About the z_m-axis ($\delta\zeta$)

In this case the incident rays remain parallel to the axis of the paraboloid. The result is a simple lateral motion of the focus, as depicted in Fig. 10. The lever arm is now R_o and the deflection simply

$$\delta y \simeq R_o\delta\zeta = r_o \sin\phi_o \ \delta\zeta \ . \tag{35}$$

Introducing the angle of incidence α, we obtain a criterion analogous to Eq. (33),

$$\delta\zeta \leq \frac{R_T \sin\alpha_{max}}{r_o \sin\phi_o} \ . \tag{36}$$

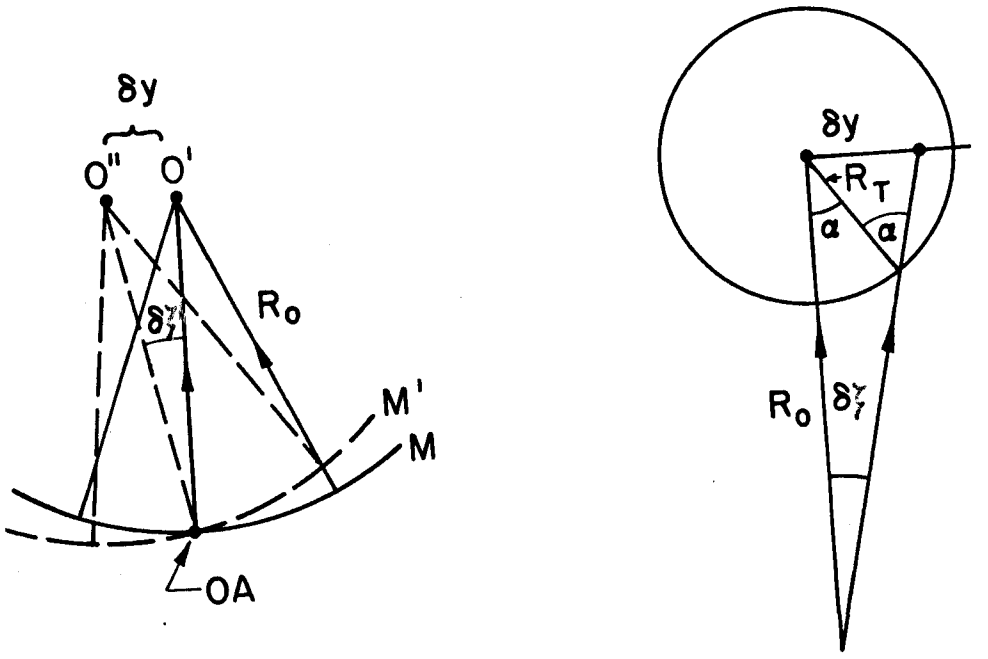

Figure 10

In this case there is some advantage in going to smaller ϕ_o.

3. Rotation About the x_m-axis ($\delta\eta$)

As before, due to the smalless of θ, we need only consider an unperturbed ray lying in the median plane. Fig. 11 is a top view of the mirror, showing how the axis of the paraboloid is rotated through the angle $\delta\eta$. The perturbed unit ray is

$$\hat{r}' = \hat{r} + 2\cos(\phi'/2)\hat{n}' \ . \tag{37}$$

In order to calculate the perturbed normal $\hat{n}'$, we introduce yet another coordinate system (x_m, y_m, z_m) centered at the point P_o where the beam axis strikes the mirror, as sketched in Fig. 12. From the figure, the Cartesian coordinates of $\hat{n}'$ are

$$\hat{n}' = (\sin(\phi/2),\ \delta\eta\cos(\phi/2),\ \cos(\phi/2)) \ . \tag{38}$$

Thus,

$$\hat{r}' = (\sin\phi,\ 2\delta\eta\cos^2(\phi/2),\ \cos\phi) \ . \tag{39}$$

The ray displacement at the focus is

$$\delta\vec{r}_m \simeq r(\hat{r}'-\hat{r}) \tag{40}$$

or

$$\delta x_m = \delta z_m = 0 \tag{41}$$

$$\delta y_m = r\ (1 + \cos\phi)\ \delta\eta = 2a\ \delta\eta$$

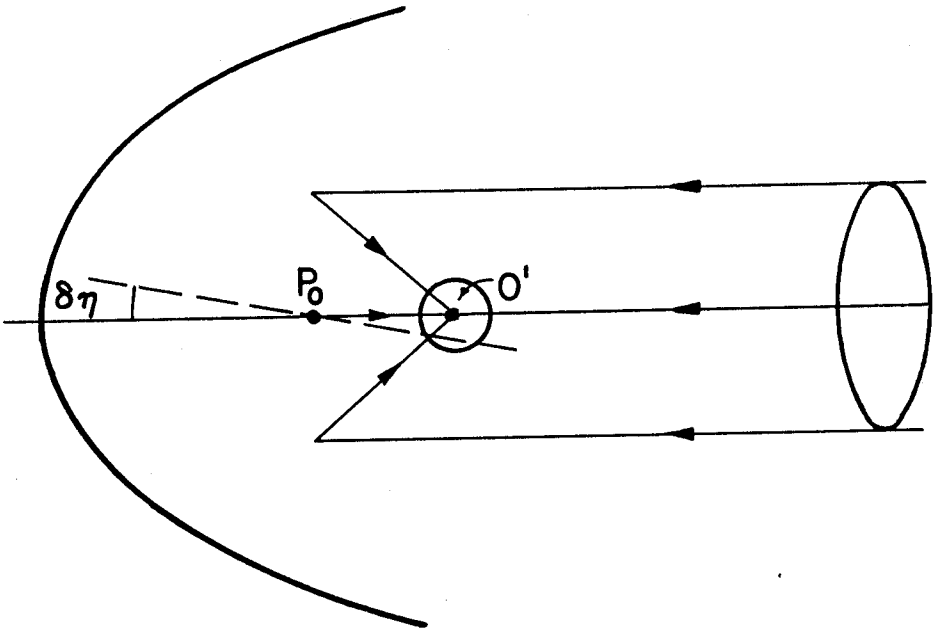

Figure 11

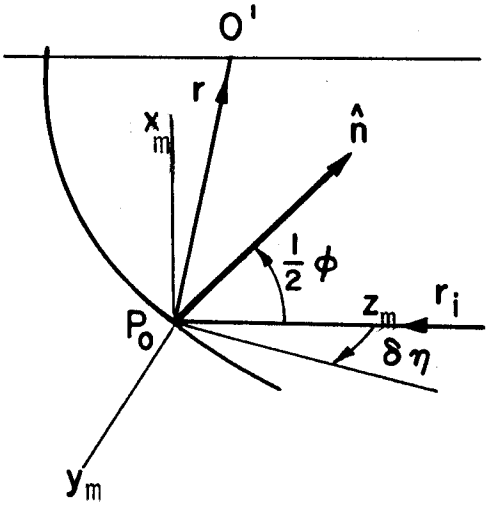

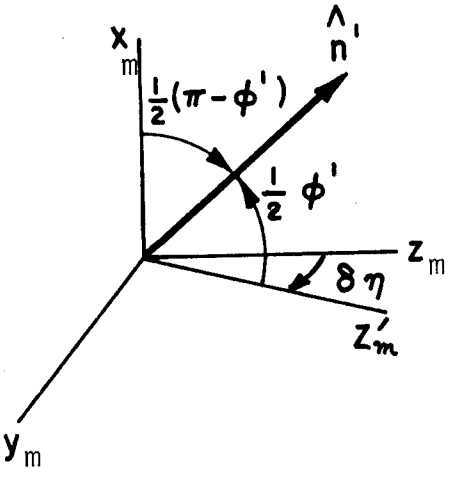

Figure 12

To impose a meaningful limit on $\delta\eta$, we again introduce the angle α:

$$\delta y = R_T \sin\alpha \ , \tag{42}$$

which gives

$$\delta\eta \leq \frac{R_T \sin\alpha_{max}}{r_o(1+\cos\phi_o)} \ , \tag{43}$$

exhibiting a rather weak dependence on ϕ_o.

In summary, we have derived the three angular constraints (pitch, roll and yaw)

$$\begin{aligned} \delta\phi &\leq \frac{R_T \sin\alpha_{max}}{2r_o} \\ \delta\zeta &= \frac{2\delta\phi}{\sin\phi_o} \\ \delta\eta &= \frac{2\delta\phi}{1+\cos\phi_o} \ . \end{aligned} \tag{44}$$

Figure 13 displays these tolerances as functions of turning angle, with $\delta\phi$ normalized to unity. The tightest tolerance is on $\delta\phi$, due to the fact that the reflected ray is perturbed by twice the tilt angle. However, note that yaw becomes equally important at small turning angles. The minimum in $\delta\zeta$ is easily understood geometrically. To get an idea of the order of magnitude of these tolerances, let R_T = 1 mm, r_o = 15 m and $\alpha = 30^o$. Then $\delta\phi$ = 16.5 μrad, or about 3 sec of arc, a reasonable design limit.

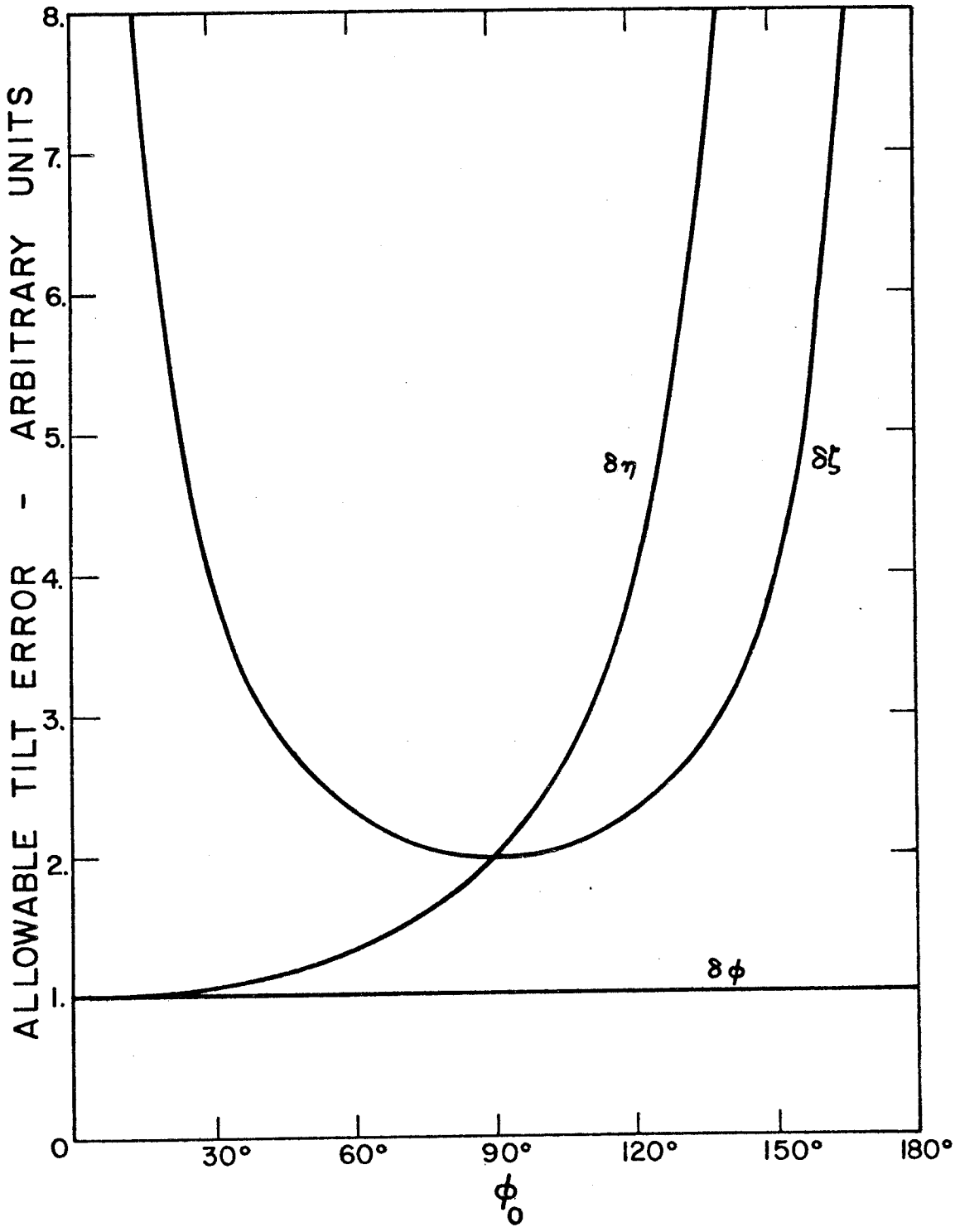
ALLOWABLE TILT ERROR - ARBITRARY UNITS
8.
7.
6.
5.
4.
3.
2.
1.
0
30°
60°
90°
120°
150°
180°
ϕ_0
$\delta\eta$
$\delta\zeta$
$\delta\phi$

Figure 13

V. Perturbed Irradiance

While it is sufficient to look at the deflection of the beam axis in estimating allowable tilt errors, more precision is called for in calculating irradiance variations over the translated spot. This calculation is greatly complicated by the fact that the perturbed rays no longer come to a sharp focus. One must then find the intersection of two contiguous rays for each value of ϕ, the locus of such points forming the caustic surface, as discussed in the Appendix. We shall restrict our attention to the perturbed irradiance under the most deleterious tilt, $\delta\phi$. The effect of the other two rotations may be found by ray tracing, if desired.

A. Target Irradiance Under the Rotation $\delta\phi$

Figure 14 illustrates the geometry required to solve this problem. Two contiguous rays intersect at the point O" in the R-z plane, having polar coordinates (ℓ,χ). As before, we invoke energy conservation

$$I_T' \, dA_T' = I_B \, dA_B \qquad (45)$$

with $dA_B = RdRd\theta$. Examination of Fig. 14 shows that the target area element is

$$dA_T' = (R_T \, d\beta) \, (\ell_1 \sin\phi') \, d\theta \ , \qquad (46)$$

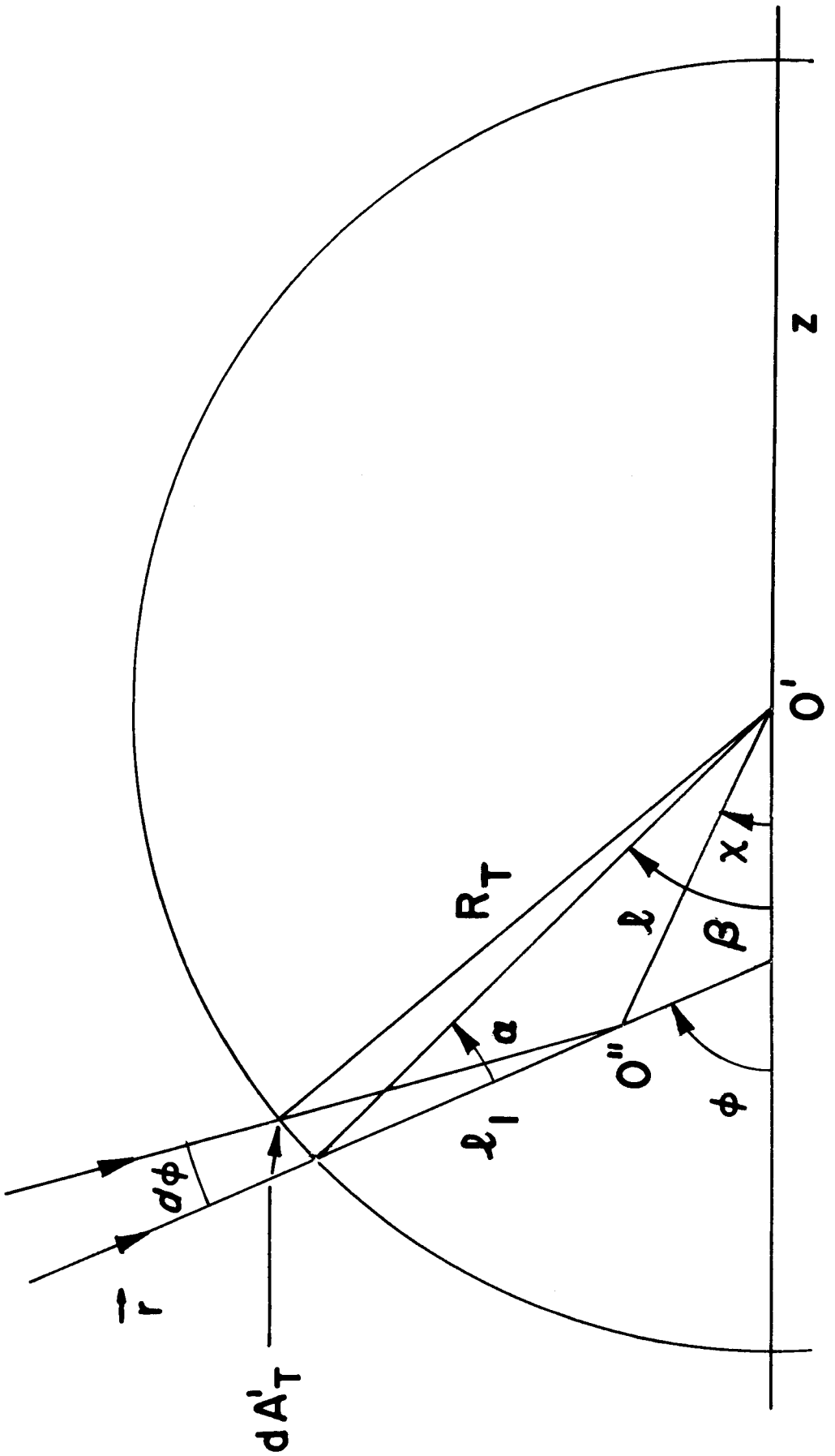

FIGURE 14

so that

$$I_T' = \frac{I_B R^2 \, d\phi/d\beta}{R_T \ell_1 \sin^2\phi} , \tag{47}$$

where Eq. (25) has been used to eliminate dR. Simple triangulation yields

$$\ell_1 \sec\alpha \, d\phi = R_T \, d\beta \tag{48}$$

$$\ell_1 \sin(\phi-\chi) = R_T \sin(\beta-\chi) . \tag{49}$$

From the Appendix,

$$\chi = \frac{3}{2}\phi - \frac{\pi}{2} . \tag{50}$$

Combining Eqs. (47)-(50) we obtain

$$I_T' = I_T \frac{\cos\alpha \cos^2(\phi/2)}{\cos^2(\alpha+\phi/2)} \tag{51}$$

where I_T is the unperturbed irradiance and α is given by

$$\sin\alpha = \frac{2r\delta\phi}{R_T} = \frac{2a\delta\phi}{R_T} \sec^2(\phi/2) . \tag{52}$$

The irradiance is infinite when the caustic intersects the pellet surface; that is, when $\chi = \beta \Rightarrow \alpha + \phi/2 = \pi/2$. From Eq. (52) we see that a hot spot occurs when

$$\delta\phi = \frac{R_T}{2a} \cos^3(\phi/2) , \tag{53}$$

provided that ϕ falls within the focal cone. In laser fusion

reactor applications ϕ varies from ϕ_o by only a few degrees, in which case Eq. (53) simplifies to

$$\delta\phi^* \simeq \frac{R_T}{2r_o} \cos(\phi_o/2) . \qquad (54)$$

For example, if r_o = 10 m, $\phi_o = 90^o$ and R_T = 1 mm, then $\delta\phi^*$ = 35.4 μrad; but if r_o = 100 m, $\delta\phi^*$ = 3.54 μrad, which might be difficult to maintain in practice.[12]

It is interesting to relate the perturbed irradiance to our tilt error criterion, $\alpha \leq 30^o$. Setting $\alpha = 30^o$ in Eq. (51) gives $I_T' = 6.5\ I_T$ for $\phi_o = 90^o$ but only $I_T' = 2\ I_T$ for $\phi_o = 45^o$. In general, larger turning angles result in less uniform, higher average irradiance. Now it is easy to show that the displacement angle corresponding to $\delta\phi^*$ is approximately $\alpha^* = \pi/2 - \phi_o/2$. (Recall that the ray misses the target when $\alpha > \pi/2$). Thus, satisfying the tilt error criterion automatically avoids the caustic when $\phi_o < 120^o$. Nevertheless, as we shall see, significant distortion of the target irradiance can take place for $\delta\phi < \delta\phi^*$.

To complete this discussion of pellet illumination near a caustic, we must express I_T' in terms of the pellet angle β (Fig. 14) rather than the ray angle. Combining Eqs. (31) and (52) we have

$$\beta = \phi - \sin^{-1}(A\sec^2(\phi/2)) , \qquad (55)$$

with

$$A \equiv \frac{2a\delta\phi}{R_T} = \frac{2r_o\delta\phi}{R_T} \cos^2(\phi_o/2) \ . \qquad (56)$$

In order to obtain $I_T'(\beta)$ we must solve Eq. (55) for $\phi(\beta)$. Unfortunately, this leads to a cumbersome quartic equation. Moreover, the mapping is double-valued. That is, when $\delta\phi$ approaches $\delta\phi^*$, a given point on the pellet surface is illuminated by two distinct ray bundles. To clarify this point, we set $d\beta/d\phi = 0$ in Eq. (55) to obtain the location of β_{max};

$$\cos(\tilde{\phi}/2) = \left(\frac{\delta\phi}{\delta\phi^*}\right)^{1/3} \cos(\phi_o/2) \ . \qquad (57)$$

It follows that

$$\beta_{max} = \frac{3}{2}\tilde{\phi} - \frac{\pi}{2} \ . \qquad (58)$$

That is, <u>the maximum pellet angle always lies on the caustic</u>. Also note that $\tilde{\phi} = \phi_o$ <u>exactly</u> when $\delta\phi = \delta\phi^*$, the critical tilt angle given only approximately by Eq. (54). An approximate expression for $\phi(\beta)$ may be obtained by Taylor expanding Eq. (55) about $\tilde{\phi}$. The result is

$$\phi \tilde{\simeq} \tilde{\phi} \pm \left[\frac{2}{3}\sin\tilde{\phi}\,(\beta_{max} - \beta)\right]^{1/2} \ , \qquad (59)$$

clearly exhibiting the double-valued character of the mapping.

To use these results for given r_o, R_T, ϕ_o and $\delta\phi$ one may proceed as follows: obtain $\delta\phi^*$ from Eq. (54), $\tilde{\phi}$ from Eq. (57) and β_{max} from Eq. (58). The target irradiance is then given by Eq. (51) summed over <u>both</u> branches of $\phi(\beta)$. If $\tilde{\phi}$ lies outside the focal cone, only one branch is to be retained. Figures 15 and 16 depict $I_T'(\beta)$ for various tilt errors with r_o = 10 m, ρ_B = 1 m, R_T = 1 mm, and $\phi_o = 45^o$ and 90^o, resp. (The angle β_{max} is out of range in all these cases). Flat beam profiles were used in all cases except one, to illustrate the dramatic smoothing effect of a Gaussian beam profile, taking α = 2 in Eq. (27). In these figures we have normalized I_T by taking I_T = 1 when $\phi = \phi_o$, as in Figs. 5-7.

Figure 17 illustrates the very large irradiances that occur near the caustic, in this case for $\phi_o = 90^o$, for which $\delta\phi^*$ = 35.4 μrad. The singularities occur at β_{max} as given by Eq. (58); the discontinuities are a result of the folding of the ray bundles about β_{max}, as discussed above. These results have been verified quantitatively by ray tracing. Thus, the extraordinarily simple equation (50) for the caustic provides a wealth of new information on pellet irradiance, previously obtainable only by machine computation.

The author's efforts to investigate the role of diffraction, however, have been frustrated by the lack of full-physical optics codes valid near caustics. It would be worthwhile to develop such a code, in lieu of quantitative guidelines for the limits of geometric optics. One can easily see, nevertheless, that the smooth structure manifested in Figs. 15 and 16 covers about 200 μm of the surface of a 1 mm radius pellet, comfortably large compared to 10 μm laser light. On the other hand, the spikes

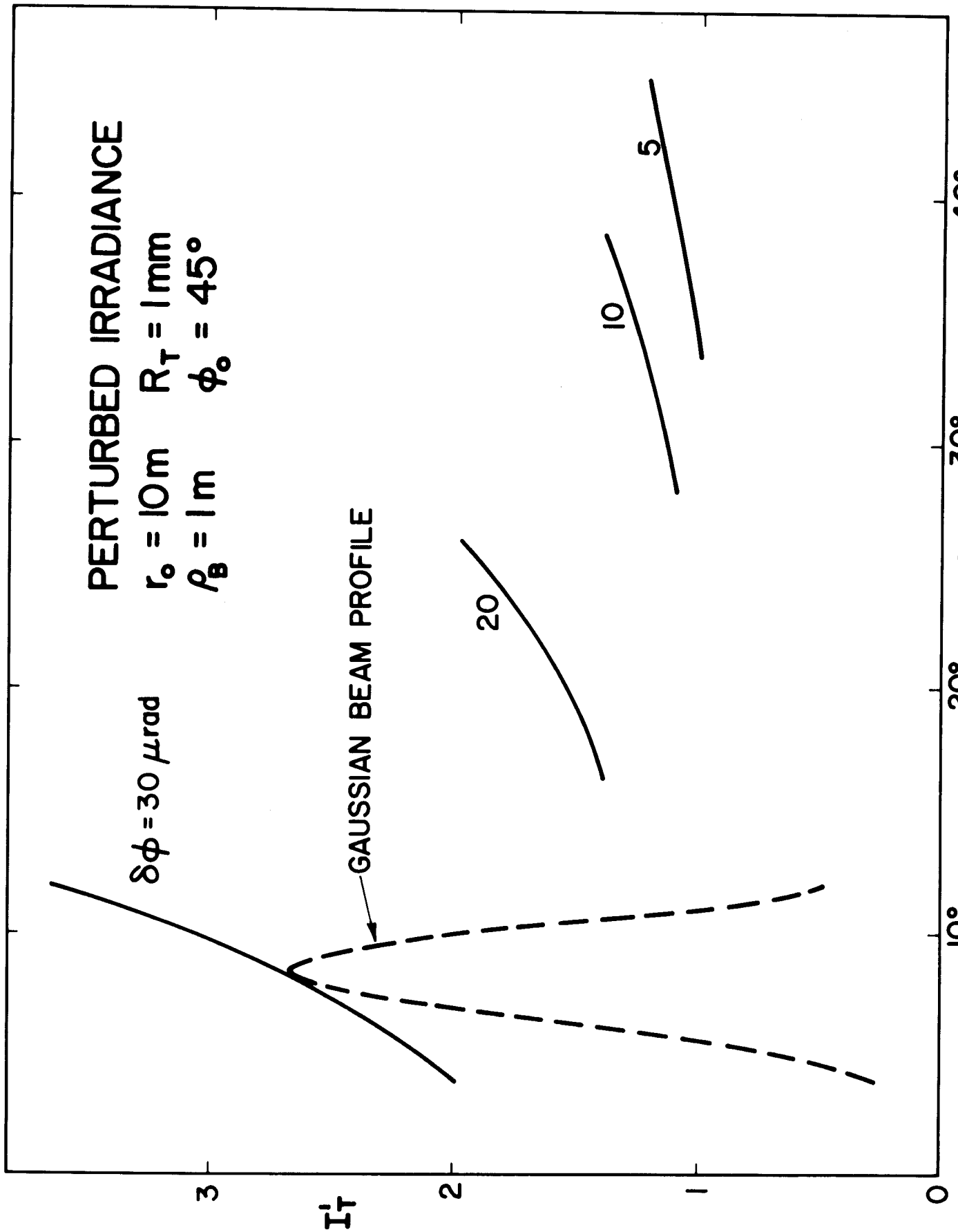
PERTURBED IRRADIANCE
r_o = 10m R_T = 1mm
ρ_B = 1m ϕ_o = 45°
$\delta\phi$ = 30 μrad
GAUSSIAN BEAM PROFILE
20
10
5
I'_T
0
1
2
3
10°
20°
30°
40°
β

FIGURE 15

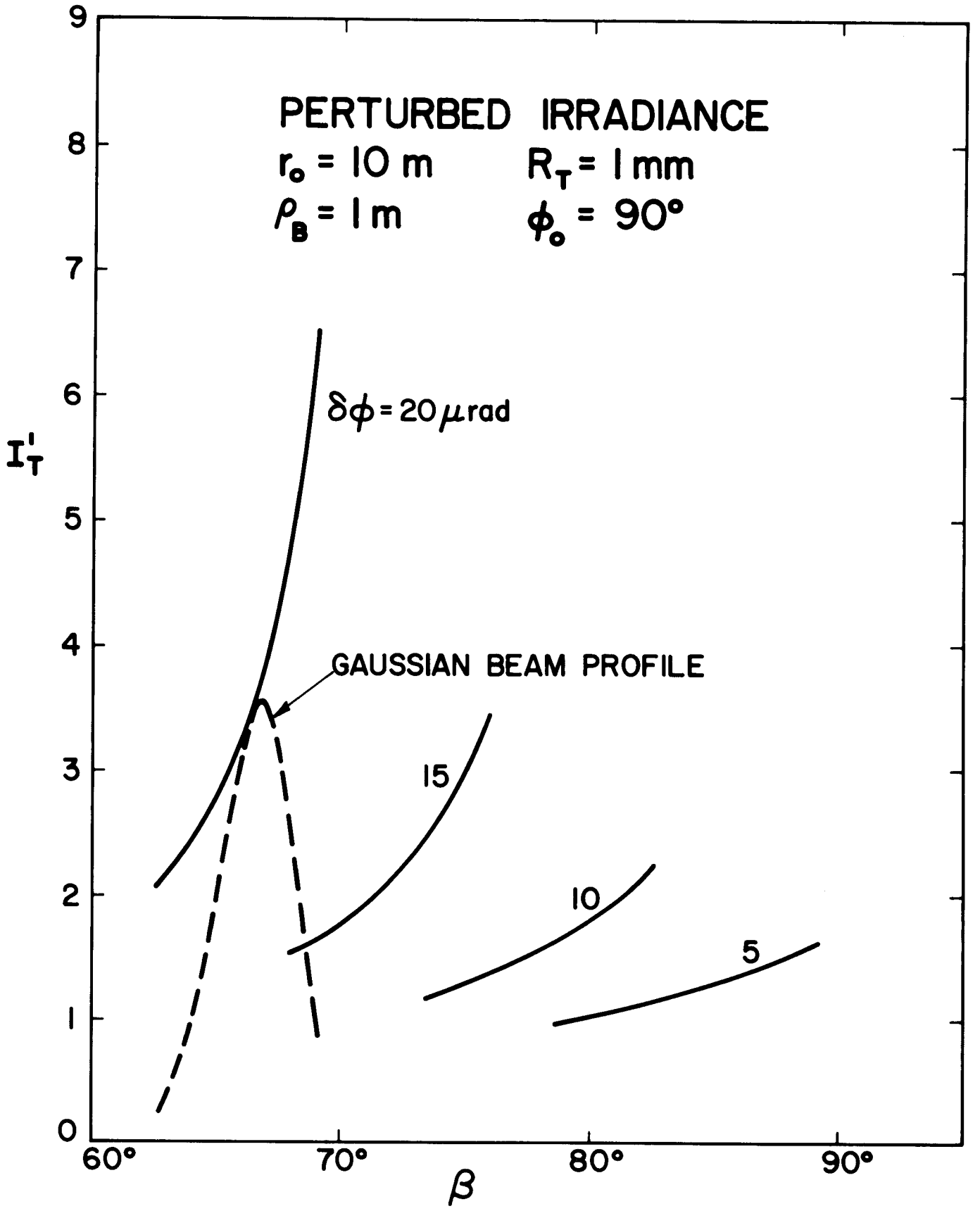
PERTURBED IRRADIANCE
r_o = 10 m
R_T = 1 mm
ρ_B = 1 m
ϕ_o = 90°
$\delta\phi$ = 20 μrad
GAUSSIAN BEAM PROFILE
15
10
5
I'_T
β
0
1
2
3
4
5
6
7
8
9
60°
70°
80°
90°

FIGURE 16

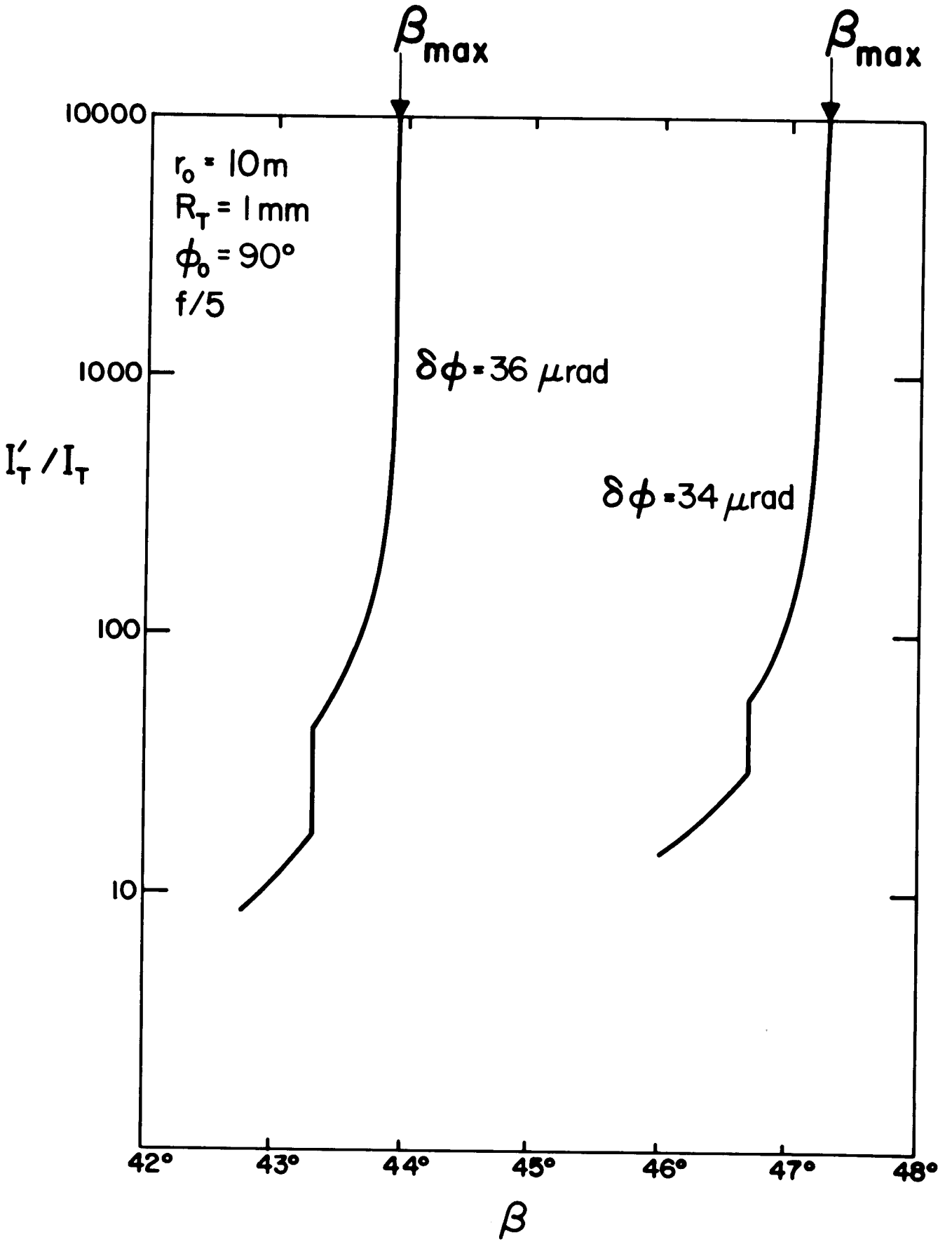
β_{max}
β_{max}
10000
1000
100
10
r_0 = 10m
R_T = 1mm
ϕ_0 = 90°
f/5
$\delta\phi$ = 36 μrad
$\delta\phi$ = 34 μrad
I'_T / I_T
42°
43°
44°
45°
46°
47°
48°
β

Figure 17

in Fig. 17 occupy only about 20 μm of the surface and will certainly be strongly modified by diffraction.

VI. Discussion

We have studied the imaging properties of far off-axis paraboloidal reflectors in the parameter range encountered in laser fusion reactor applications. The shape of the image disk was calculated analytically by means of an expansion in powers of inverse off-axis f/no. and was found to be a shifted circle in lowest order. The f/no. itself was shown to be nearly independent of turning angle for large f/no. Closed form expressions were derived for the irradiance cast on a spherical target centered at the mirror focus. Excellent agreement was found between numerical calculations and the analytic formulas. The asymmetry of the target irradiance was found to increase with decreasing f/no. and increasing turning angle (large turning angles necessitate excessively large mirrors).

The effect of various tilt errors on the focus was also exhibited, first by calculating ray deflections and then by a detailed examination of the perturbed target irradiance. Maximum allowable roll, pitch and yaw tilts were shown to depend differently on turning angle, with pitch being the most restrictive motion. An analytic expression was derived for the perturbed target irradiance under a small pitch angle tilt, based on a new calculation of the caustic curve. This calculation also yielded a simple criterion for the caustic to intersect the target surface.

The question naturally arises as to the choice of a practical design limit for the tilt error in an actual laser fusion reactor, rather than experimental facilities such as SHIVA[10] and ANTARES.[11] The final turning mirrors in SHIVA are controlled to within ± 1 μrad, while the ANTARES mirrors are held to within ± 10 μrad. The principal reason for the smaller tolerance for SHIVA is that it was originally intended to provide uniform illumination (now defunct). The larger value allows less stringent optical tolerances with considerable savings in cost. The present study shows that tilt errors of ± 10 μrad do not severely affect target irradiance, except for very long (~ 100 m) focal length systems.[12] A more detailed study of a conceptual laser fusion reactor will be presented elsewhere.[13]

Finally, we would like to emphasize the crucial role of the initial beam profile in shaping target irradiance. A flat top beam profile, typical of saturated laser amplification, produces the maximal asymmetry, while a radially decreasing profile, characteristic of an unsaturated laser medium, can have a strong smoothing effect. Gas phase lasers can operate near saturation, but glass rod/slab lasers must run at lower intensities in order to avoid self-focusing damage. In a commercial reactor one would naturally seek to operate as near saturation as possible to ensure high system efficiency. Thus, tilt error control will be of paramount importance in the design of a laser fusion reactor.

Appendix: Caustic for Tilted Paraboloid

Consider the paraboloid

$$R^2 = 4az \tag{A1}$$

with rays incident at angle $\delta\phi$ with the axis of symmetry, as depicted in Fig. A1. (We have now taken the origin to be the vertex of the paraboloid).

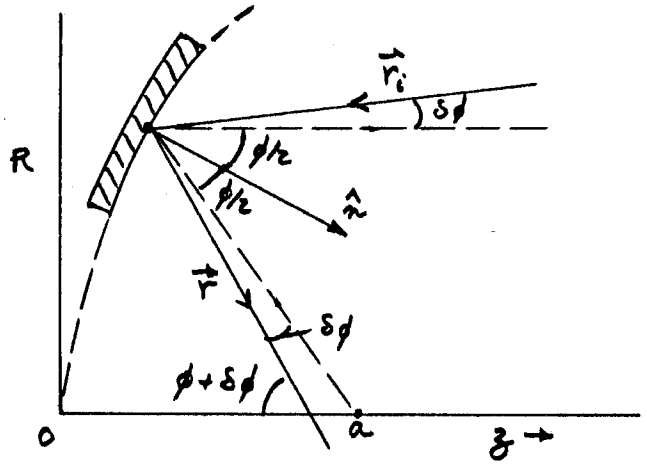

Figure A1

The caustic is formed by the intersections of the reflected rays $\vec{r}$, with either ϕ or R taken as variable parameter and $\delta\phi$ fixed. The reflected ray is given by

$$R - R_0 = - (z - z_0) \tan (\phi + \delta\phi) , \tag{A2}$$

where R_0 and z_0 are the coordinates of the ray-mirror intersection point. Using $R_0 = 2a \tan(\phi_0/2)$, we find

$$F(R,z,\phi,\delta\phi) = R - 2 \tan(\phi/2) + (z - \tan^2(\phi/2)) \tan (\phi + \delta\phi) = 0 , \tag{A3}$$

where a has been scaled out. The envelope equation is[8]

$$\frac{\partial F}{\partial \phi} = 0 , \tag{A4}$$

which yields

$$\cos^2(\phi/2)(z - \tan^2(\phi/2)) = \cos^2(\phi + \delta\phi)\,[1 + \tan(\phi/2)\,\tan(\phi + \delta\phi)] \quad \text{(A5)}$$

$$R = 2\tan(\phi/2) - (z - \tan^2(\phi/2))\,\tan(\phi + \delta\phi)\ . \quad \text{(A6)}$$

The caustic may be obtained by eliminating ϕ between Eqs. (A5) and (A6). As a check note that the trivial solution $R = 0$, $z = 1$ results for $\delta\phi = 0$. The general solution has been obtained by Stalzer.[9] The result may be written

$$27t(\Delta z - Rt)^2 = (R + zt)\,(R - 8t + t\Delta z)^2\ , \quad \text{(A7)}$$

where $\Delta z \equiv z - 1$ and $t \equiv \tan(\delta\phi)$. However, since $\delta\phi \ll \delta$ is always well satisfied in laser fusion applications, we may Taylor expand (A6) and (A7) to obtain

$$R \cong \frac{2(1 - 2\cos\phi)}{1 + \cos\phi}\,\delta\phi \quad \text{(A8)}$$

$$\Delta z \cong -\frac{2\sin\phi(1 + 2\cos\phi)}{(1 + \cos\phi)^2}\,\delta\phi\ . \quad \text{(A9)}$$

Eliminating ϕ between (A8) and (A9) yields

$$\Delta z \cong -\frac{\sqrt{3}}{9}(8 - R)\,(1 + R)^{1/2}\ , \quad \text{(A10)}$$

where $\delta\phi$ has been scaled out. This expression agrees with Stalzer's result (A7) in the limit $\delta\phi \to 0$. Eq. (A10) is plotted in dimensionless form in Fig. A2. The left hand portion is due to rays re-

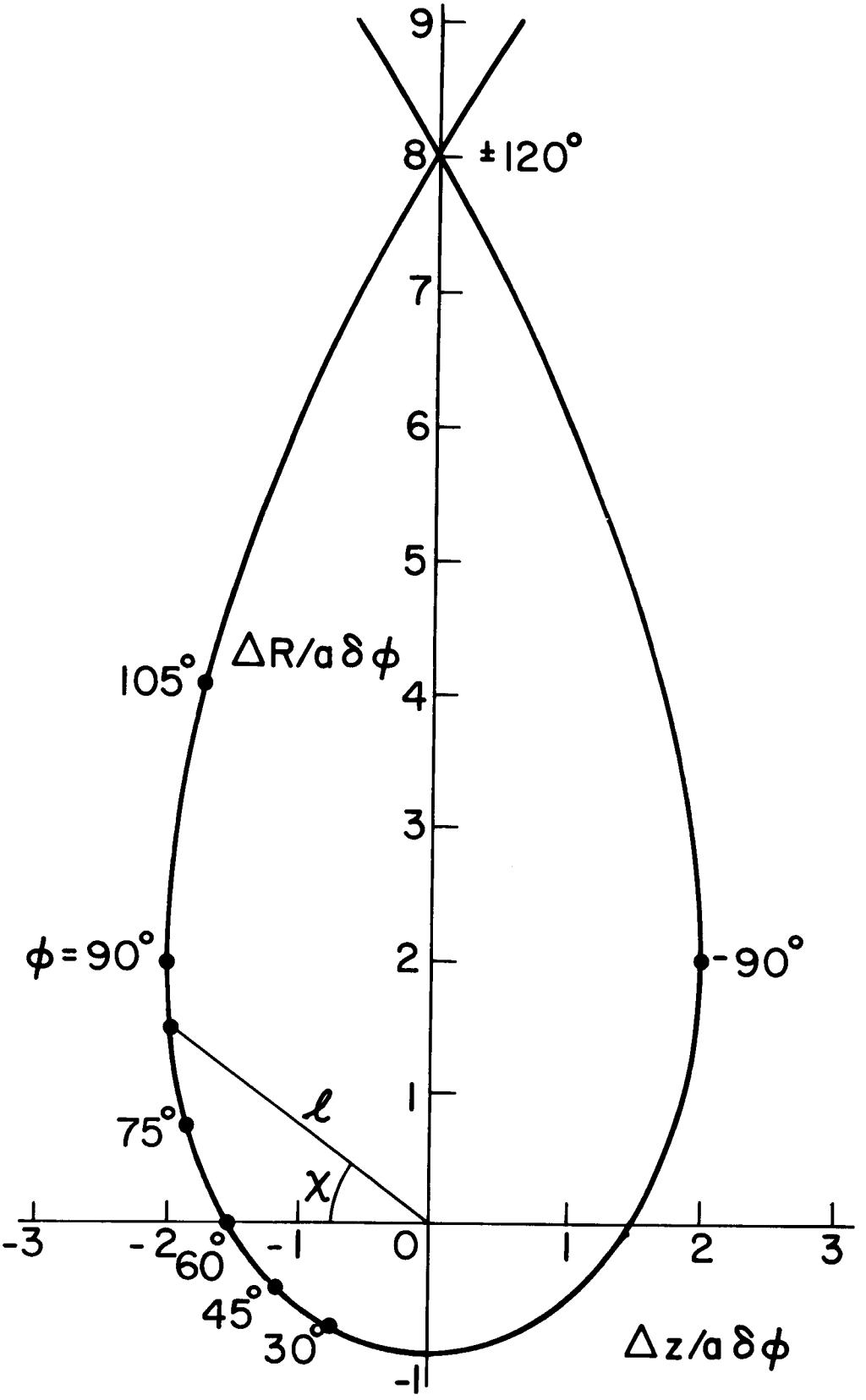

FIGURE A2

flected from the upper portion of the mirror depicted in Fig. A1 and the right hand portion is produced by the lower half (if a complete mirror is present).

In applying these results to the design of a laser fusion illumination system, one would seek to keep $a\delta\phi$ sufficiently small that the caustic would fall entirely inside the (spherical) target. Figure A3 shows the caustics produced by tilt errors of $\pm$ 25 μrad for a paraboloid with paraxial focal length a = 5m, superimposed on a target 1 mm in radius (with $\delta\phi$ doubled because we are tilting the mirror rather than the beam). While the caustic is entirely interior to this pellet for all turning angles of interest ($\phi \leq 90^{o}$), a hot spot would be produced on a smaller target wherever the caustic intersects the surface.

The caustic Eq. (A10) takes a simple and useful form in polar coordinates (ℓ,χ) as illustrated in Fig. A2. We find

$$\ell = a\delta\phi \sec^3 (\phi/2) \tag{A11}$$

$$\chi = \frac{3}{2}\phi - \frac{\pi}{2} , \tag{A12}$$

so that the caustic becomes

$$\ell = a\delta\phi \sec^3 \left(\frac{\chi}{3} + \frac{\pi}{6}\right) . \tag{A13}$$

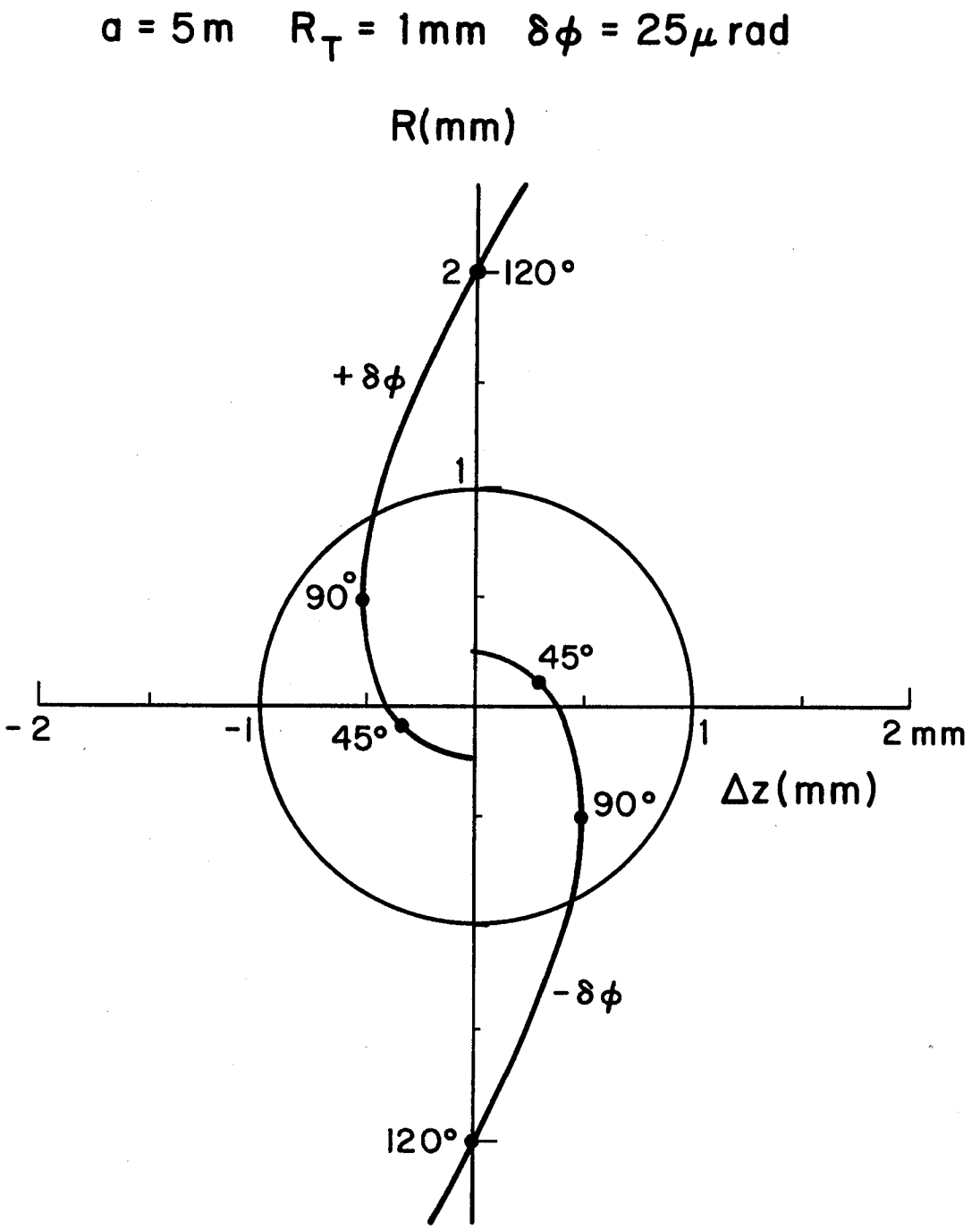

FIGURE A3

It has been shown by E.J. Guay[14] that the caustic for arbitrarily large tilt angle may be obtained by replacing $\delta\phi$ with sin $\delta\phi$ in Eq. (A13). Finally we note that if the mirror is tilted instead of the beam, $\delta\phi$ must be replaced by $2\delta\phi$ in Eqs. (A11) and (A13).

Acknowledgements

It is a pleasure to thank Prof. A. D. Code for helpful discussions. This work was supported by the Electric Power Research Institute.

References

1. W. H. Reichelt, D. J. Blevins and W. C. Turner, Los Alamos Scientific Lab. Report LA-UR 77-468.
2. T. T. Saito, Applied Optics 14, 1773 (1975).
3. R. W. Conn, et al., Fusion Research Program Report UWFDM-220, Univ. of Wisconsin (December 1977).
4. J. A. Maniscalco, Lawrence Livermore Lab. Report UCRL-78682, September 1976.
5. H. P. Brueggemann, Conic Mirrors, Focal Press Limited (London), 1968.
6. Ref. 3, Sec. V-C.
7. S. S. Glaros and A. J. Glass, Sixth Symposium on Engineering Problems of Fusion Research, San Diego, November 1976, p.
8. J. Morgan, Introduction to Geometrical and Physical Optics, McGraw-Hill (New York, 1953), p. 420.
9. H. J. Stalzer, Jr., Applied Optics 4, 1205 (1965).
10. E. S. Bliss, et al., Bull. Am. Phys. Soc. 22, 1158 (1977).
11. W. H. Reichelt, private communication.
12. M. J. Monsler and J. A. Maniscalco, Lawrence Livermore Lab. Report UCRL-79990 (November 1977).
13. J. E. Howard, University of Wisconsin FRP Report UWFDM-238 (March 1978).
14. E. J. Guay, private communication.

FIGURE CAPTIONS

Fig. 1. Parabolic mirror imaging geometry. A circular beam is shown incident from the right, parallel to the mirror symmetry axis OO'. The effective focal length of the off-axis mirror is r_0 at the principal ray height R_0. In practice the parameter $\underline{a}$ is determined by r_0 and the turning angle ϕ_0. The effective off-axis f/no. depends on r_0 and the beam radius ρ_B, independent of ϕ_0.

Fig. 2. Image of a circular beam, in a plane normal to $\vec{r}_0$ at distance $r_0^* < r_0$ from focus O'. ρ_1' and ρ_2' are the limits of the image contour in the median plane.

Fig. 3. Transformation to beam-centered coordinates. The z axis has been rotated through the angle ϕ_0 in the median plane. The new z axis $\tilde{z}$ coincides with the beam axis along $\vec{r}_0$, while the y axis is unchanged.

Fig. 4. Image contour for large f/no. To lowest order in ε the image is a circle of radius ε, with the beam axis shifted by an amount $\Delta\xi$ in the $-\phi$ direction.

Fig. 5. Irradiance profiles for a flat beam profile and focal length $r_0 = 5\ \rho_B$. Profiles are shown for turning angles $\phi_0 = 45^o$, 90^o and 135^o in the median plane.

Fig. 6. Irradiance profiles for a Gaussian beam falling off by one e-folding.

Fig. 7. Irradiance profiles for a Gaussian beam falling off by two e-foldings.

Fig. 8. Geometry of a ray when the parabolic mirror is tilted through $\delta\phi$ in the median plane (rotation about the y_m axis). Perturbed quantities are denoted by primes.

Fig. 9. Tilt error criterion. The location of the perturbed ray is limited to the angle α_{max} measured from the target center.

Fig. 10. Tilt error geometry for rotation of the mirror through $\delta\zeta$ about the z axis, coincident with the beam axis (roll).

Fig. 11. Tilt error geometry for rotation of the mirror through $\delta\eta$ about the x_m axis (yaw).

Fig. 12. Details of rotation about x axis. The normal $\hat{n}$ lies in the x_m-z_m plane, while the perturbed normal $\hat{n}'$ lies in the x_m-z_m' plane.

Fig. 13. Normalized roll, pitch, and yaw tolerances as a function of turning angle ϕ_o.

Fig. 14. Perturbed target irradiance geometry. Two neighboring rays intersect at point O", which lies on the caustic. Points on the caustic are given in polar coordinates (ℓ,χ), as described in the Appendix.

Fig. 15. Perturbed target irradiance for turning angle $\phi_o = 45^o$ and small tilt errors. Note that the range of β decreases with increasing $\delta\phi$. Flat beam profiles are assumed; a Gaussian profile ($\alpha = 2$) is used in one case to show its strong smoothing effect. The unperturbed irradiance I_T varies by 18% for a flat beam profile.

Fig. 16. Perturbed target irradiance for turning angle $\phi_o = 90^o$ and small tilt errors. In this case I_T varies by 49%.

Fig. 17. Perturbed target irradiance in the vicinity of the caustic, with $\phi_o = 90^o$ and $\delta\phi^* = 35.4$ μrad. The discontinuities are due to overlapping ray bundles. The spikes at β_{max} would be strongly modified by diffraction.

Fig. A1. Mirror-target geometry with incident ray at a small angle $\delta\phi$ with the mirror axis. This convention is chosen to agree with the literature on caustics.

Fig. A2. Full caustic curve for a paraboloidal mirror.

Fig. A3. Caustic for paraboloidal mirror superimposed upon a 1 mm radius target. The two separate branches correspond to positive and negative tilts using the upper half-mirror alone. Note that since the latus rectum is held constant here, the focal length will vary with ϕ. In the numerical examples in Sec. V, r_o is held constant and a varied.